

Article

Photovoltaic-Based q-ZSI STATCOM with MDNESOGI Control Scheme for Mitigation of Harmonics

Kanagaraj Nallaiyagounder ^{1,*}, Vijayakumar Madhaiyan ², Ramasamy Murugesan ² and Obaid Aldosari ¹

¹ Electrical Engineering Department, College of Engineering in Wadi Al-Dawasir, Prince Sattam Bin Abdulaziz University, Al-Kharj 11991, Saudi Arabia; om.aldosari@psau.edu.sa

² Department of Electrical and Electronics Engineering, K.S.R. College of Engineering, Tiruchengode, Namakkal 637215, Tamilnadu, India; vijayakumar1@ksrce.ac.in (V.M.); ramasamy@ksrce.ac.in (R.M.)

* Correspondence: thirukanagaraj@yahoo.com or k.gonder@psau.edu.sa

Abstract: Static compensators (STATCOMs) are often used in distribution systems to enhance power quality. There is a need to enhance the performance of STATCOM to optimize its utilization and facilitate the provision of additional ancillary services. This paper employs the multilayer discrete noise-eliminating second order generalized integrator (MDNESOGI) to regulate the quasi-impedance source inverter (qZSI)-STATCOM for power exchange with the grid. Compared to conventional second-order generalized integrator (SOGI), MDNESOGI exhibits a higher capability for rejecting DC offset. In instances of abnormal grid operation or system malfunction, the inclusion of DC rejection capability enhances the robustness and reliability of the system. The suggested control algorithm only requires two integrators, three mathematical operators, and a damping factor, making it far easier to implement than transformation-based methods. The distorted load current is broken down into its active and reactive components using this control mechanism. The reference currents are then calculated by multiplying these parts by their corresponding voltage standards. The DC offset is reduced and transient oscillations in the weight component are eliminated by adjusting the damping factor. The suggested algorithm effectively handles power quality tasks like (a) reducing harmonic distortion, (b) compensating for reactive power, (c) adjusting for power factor, and (d) balancing the load under different conditions in the distribution system. The experimental study results are used to examine the stability of the proposed control scheme in both static and dynamic scenarios. In addition, a comparison to traditional methods is provided to demonstrate the new method's superiority. Experimentation results show that the suggested controller is superior to its contemporaries in all scenarios where power quality is a factor, meeting the IEEE standard requirements.

Keywords: multilayer discrete noise-eliminating second order generalized integrator; static compensators; power quality; DC rejection capability; PV system



Citation: Nallaiyagounder, K.; Madhaiyan, V.; Murugesan, R.; Aldosari, O. Photovoltaic-Based q-ZSI STATCOM with MDNESOGI Control Scheme for Mitigation of Harmonics. *Energies* **2024**, *17*, 534. <https://doi.org/10.3390/en17020534>

Academic Editor: Santi A. Rizzo

Received: 7 December 2023

Revised: 11 January 2024

Accepted: 18 January 2024

Published: 22 January 2024



Copyright: © 2024 by the authors. Licensee MDPI, Basel, Switzerland. This article is an open access article distributed under the terms and conditions of the Creative Commons Attribution (CC BY) license (<https://creativecommons.org/licenses/by/4.0/>).

1. Introduction

Power utilities that rely on fossil fuels are becoming phased out in favour of renewable energy sources (RES) as a result of increasing carbon emissions and the growing demand for energy on a global scale. Since solar energy can be accessed from a greater geographical region and can be transformed directly into electricity via the use of photovoltaic (PV) panels, it is the renewable energy source that is utilized the most around the globe [1]. Concurrently, several power quality (PQ) problems have arisen due to the widespread use of power electronics, which introduces nonlinear, unbalanced, and inductive loads into the distribution network [2]. The presence of these may have a detrimental impact on electrical systems, resulting in problems such as overloading, increased losses, inadequate power factor, malfunctioning of protective devices and control circuits, and other related difficulties [3–7]. A wide range of occurrences—such as lightning, faults, short circuits, and the cycling on and off of large loads and capacitor banks—have the potential to cause

disruptions to the power grid. Changes in the voltage of the utility grid, such as sag, swell, and interruptions, are among the most-often-observed grid-side reliability problems. When problems or disruptions occurred in the past, it was necessary to temporarily disengage RESs from the network [8]. However, as additional renewable energy sources were added to the grid, the general stability of the system was put in jeopardy. If important loads were disabled as a result of voltage changes in the system, significant economic losses may conceivably ensue. In situations when the load and the grid are not in equilibrium, it is a difficult problem to maintain the stability of the system and the quality of the electricity [9].

During changeable DC link voltage situations, active power filters (both shunt and series) are used to enhance power quality under distorted and unbalanced non-linear loads. Additionally, these filters are utilized to relieve difficulties that are produced by sag and swell. PV power injection into the distribution network is another method that is utilized. On the other hand, it should be highlighted that the aforementioned active power filters (APFs) have limited capabilities because they are intended to solve just two or three separate power quality concerns and do not offer multifunctionality [10,11]. Therefore, the inverter may be used as a multipurpose device to improve power quality while simultaneously injecting photovoltaic energy into the utility grid in the case that there are concurrent imbalances in both the grid and the load. With the assistance of signal decomposition methods, it is possible to extract current values that are either unbalanced or distorted from load/source signals [12,13]. The literature has studied several time-domain control approaches for three-phase APFs. Specifically, under distorted/unbalanced grid settings, the main goals here are to estimate the reference voltage and current amounts needed for APF operation and control, and to extract the frequency, phase angle, and positive and negative sequence components [14]. Furthermore, traditional frequency-locked loops (FLLs) and low-pass filters (LPFs) are often used for reference quantity estimation, however, they both have poor performance when dealing with unbalanced and distorted signals. Power distributions that are balanced, imbalanced, or distorted all make use of enhanced instantaneous power theory (EIP) [15].

To solve this issue, a three-phase distribution network has used the synchronous reference frame (SRF) and d-q theory. However, this theory works best in a perfectly balanced three-phase network with no load, and the current generation process is disrupted by even a small amount of unbalancing in the network. To address the nonlinearity introduced by end users, STATCOM controllers based on the Lyapunov function have been developed for use in harmonic compensation. In hydropower generation, STATCOM is being used with instantaneous reactive power theory (IRPT) [16]. The battery energy storage (BES) with STATCOM is now the superior choice for enhancing power quality. To improve the dynamic reaction time of STATCOM, a phase-locked loop (PLL)-based control approach has been devised that eliminates the need for a voltage-controlled oscillator (VCO) [17]. Distribution system power quality has been enhanced by the usage of this control method. The standard SOGI approach to STATCOM has been described. This method was often used to determine the basic component of the load current and to generate the reference supply current. Load current has DC offsets because of this regulation. The dual SOGI method has been modified to take advantage of four integrators, and a method based on six integrators has also been published. These methods may reduce total harmonic distortion (THD), but they need a greater investment in integrators and hence make the system more difficult and expensive to operate [18]. For the purpose of providing long-term current-based compensation and integrating it into the utility grid, the qZSI-based STATCOM that incorporates a PV system is presented. The suggested controller may be used in the distribution system for qZSI-STATCOM control, where it will improve power quality by eliminating harmonics in the source current. The suggested structure's main characteristics are as follows:

1. The suggested architecture improves upon the existing SOGI approach by connecting two analogous filter loops for prominent harmonic components in parallel with the prime loop.

2. The suggested structure necessitates a reduced sampling time requirement, hence facilitating expedited creation of reference currents across diverse operating conditions.
3. Power quality challenges including reactive power, load balancing, power factor, and DC link voltage stabilization are addressed using the established technique.
4. The suggested architecture is developed, and its performance is evaluated and verified in the laboratory on a real-time platform.

2. Related Works

This research focuses on both static and dynamic hosting capacity (SHC and DHC) in distribution grids, and it presents an adaptive controller for static synchronous compensators to manage both steady-state and dynamic voltage without introducing any surplus reactive power [19]. The use of an artificial neural network (ANN) to evaluate the STATCOM's gain settings improves the wind farm's stability performance. To determine how tuned STATCOM affects combined wind farm (CWF) performance under gust wind speed and three-phase fault conditions, an extensive analysis is carried out [20]. The agent is trained to acquire the adaptive robust control strategy for the STATCOM-Additional Damper Controller (ADC) (Kansai Electric Power Company, Osaka, Japan) using the deep deterministic policy gradient (DDPG) technique. The suggested system has self-learning characteristics, which sets it apart from other control methods. Furthermore, the agent-generated parameter configurations for a given system operational state are valid and transportable to other states [21]. This research proposes two optimization approaches—ant colony optimization (ACO) and particle swarm optimization (PSO)—to enhance STATCOM's dynamic performance. The goal of applying these approaches to the adjustment of PI controller coefficients is to efficiently manage STATCOM dynamics [22]. We enhanced the performance of the STATCOM control circuit in a solar-wind hybrid microgrid by optimizing the gain parameters of four PI controllers. This optimization is achieved through the utilization of genetic algorithms (GA) and bacteria foraging algorithms (BFA). The suggested strategy aims to improve the system's responses and voltage stability, taking into consideration the nonlinear characteristics of the microgrid [23]. To select the ideal parameters for the basic controller used in the STATCOM control scheme, an innovative meta-heuristic swarm optimization method known as bacterial foraging optimization algorithm (BFOA) based optimum controller is suggested [24].

The integration of high levels of PV systems into the electric grid has presented novel challenges, including issues related to reverse power flow and the violation of voltage profiles. A fault classification mechanism based on support vector machines is developed to enhance the efficiency of grid fault identification [25]. A synchronverter-based PV system has been developed by STATCOM (PV-STATCOM) to enable active and reactive power exchange with the grid. The synchronverter's ability to manage the system's frequency and voltage by simulating inertia is the main differentiating factor between it and traditional control [26]. Table 1 shows the review summary of STATCOM control schemes.

Table 1. Review summary of STATCOM control schemes.

Design Approach	Control Technique	Remarks
Adaptive law [20]	Adaptive Control	The performance of the controller is contingent upon the state of the system.
ANN [21]	Soft computing	It takes a lot of time and energy to train an agent and fine-tune the control parameters.
DDPG [22]	Soft computing	The process of agent training and control parameter tuning necessitates a substantial investment of time and effort.
ACO and PSO [23]	Soft computing	The procedure of tuning requires additional time.
GA and BFA [24]	Soft computing	Tuning is a time-consuming procedure.

Table 1. Cont.

Design Approach	Control Technique	Remarks
BFA [25]	Soft computing	The design of the controller is founded upon the utilization of a linearized model or an equivalent circuit.
Coordinated control of STATCOM and PV inverter [26]	Coordinated control	The complexity of computations arises from the utilization of SVM for fault classification.
Synchronverter-based PV system [27]	Synchronverter	Need improvement in dynamic characteristics.

3. System Description

The power circuit configuration of the proposed qZSI-STATCOM is shown in Figure 1. The power circuit of the STATCOM comprises a three-leg qZSI with a shared DC connection, a PV system, and an MDNESOGI-based current and voltage controller. Through the use of an MDNSOGI-based controller, the major objective of the qZSI-STATCOM is to introduce the desired amount of active and reactive electricity into the utility grid [27,28]. Among the various components that make up the photovoltaic power generating system are the PV array, the voltage-doubler boost converter, the bidirectional buck-boost DC-DC converter, and the battery bank. Both the process of charging and draining the battery are carried out with the assistance of the bidirectional buck-boost converter. In the event that the photovoltaic system generates a substantial quantity of power, the excess energy is stored in a device that serves as a backup source of energy. This stored energy may then be used during periods of voltage interruption and reduced sunlight availability, such as overcast sessions. The voltage-doubler boost converter is responsible for regulating the DC connection of the STATCOM.

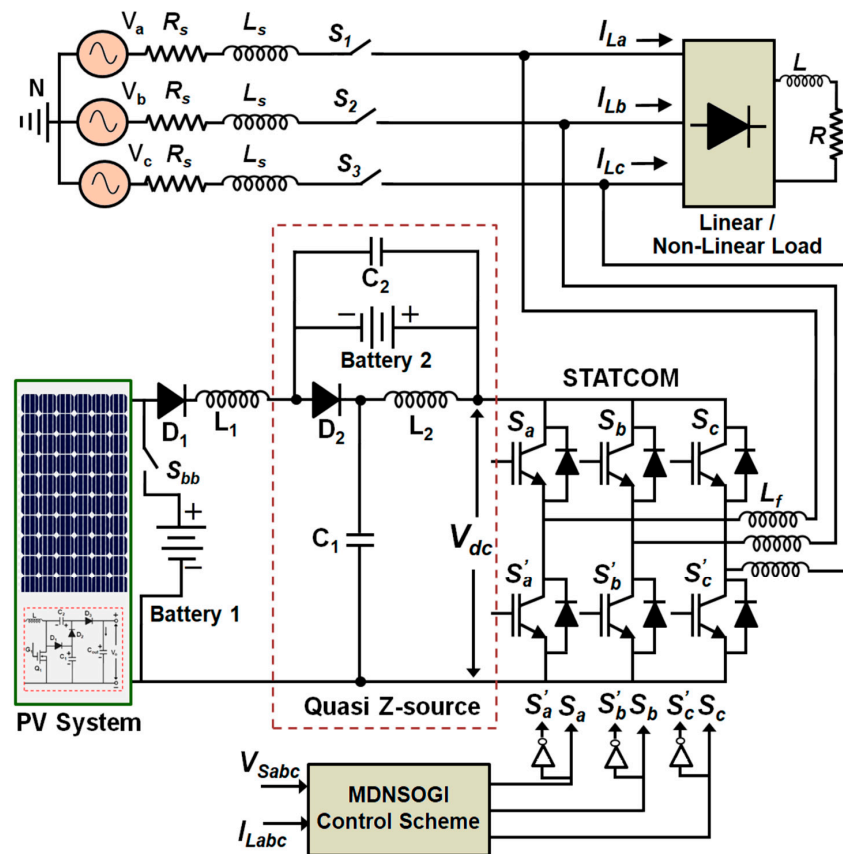


Figure 1. The configuration of the power circuit for the qZSI-STATCOM.

The PV system serves as a viable option for electricity provision, particularly in remote areas, owing to its notable attributes including minimal maintenance needs, exceptional dependability, extended lifespan, and consistent performance facilitated by stationary components. Figure 2 illustrates the photovoltaic power generation system integrated with a voltage-doubler boost converter.

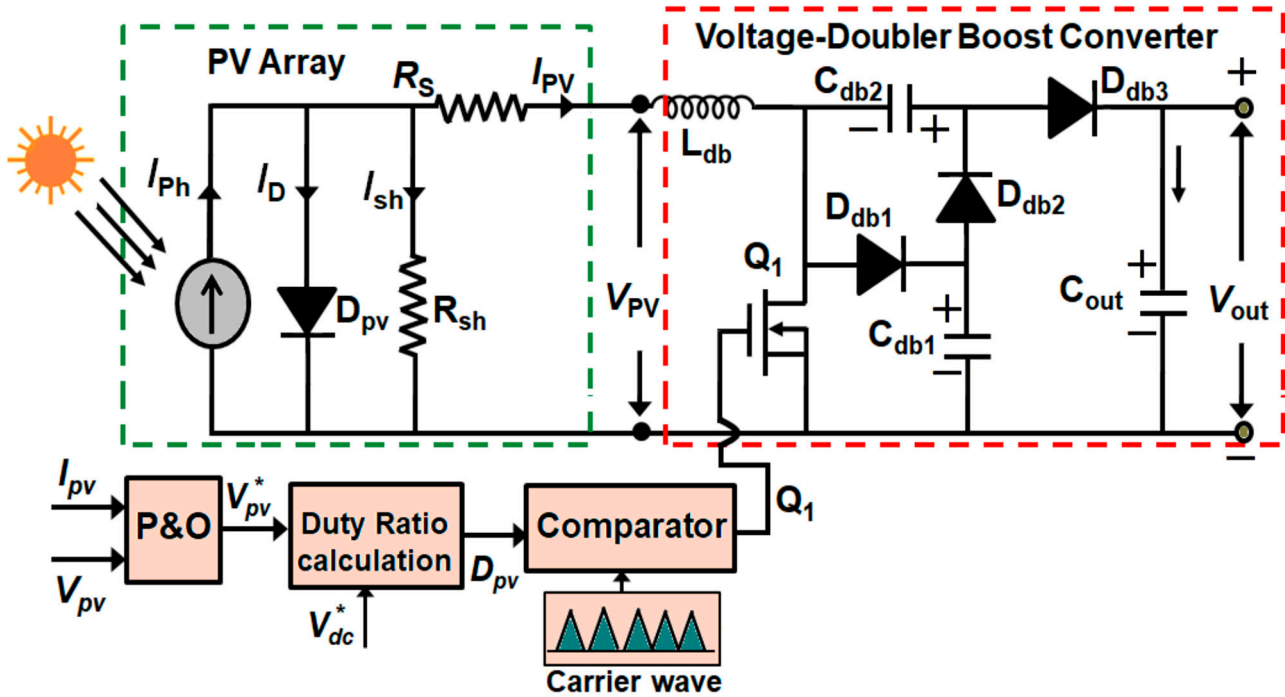


Figure 2. Photovoltaic power generating system that incorporates a voltage-doubler converter.

4. Different Operating Modes of PV-Based qZSI-STATCOM

The PV-based qZSI-STATCOM is capable of running in several operating modes, which are determined by monitoring the status of key parameters such as P_{PV} , source voltage (V_{Sabc}), P_{Load} , and state of charge of the battery (SOC). In the voltage approach, a measurement of the battery voltage is converted to the equivalent SOC value by making use of the discharge curve of the battery, which is known to be the relationship between voltage and SOC. The PV-based qZSI-STATCOM demonstrates effective multimode capability in effectively addressing power quality concerns and facilitating the sharing of active and reactive power across various operational scenarios.

4.1. Mode: 1

If the power generated by the photovoltaic system (P_{PV}) is more than or equal to the power required by the load (P_{Load}) and the SOC of the battery is less than or equal to 50%, the mode selector will choose for the PV power generating mode. This operational mode provides active power to the load that is connected, while simultaneously charging the battery by the activation of switch S_{bb} . Figure 3 shows the flowchart for Mode 1.

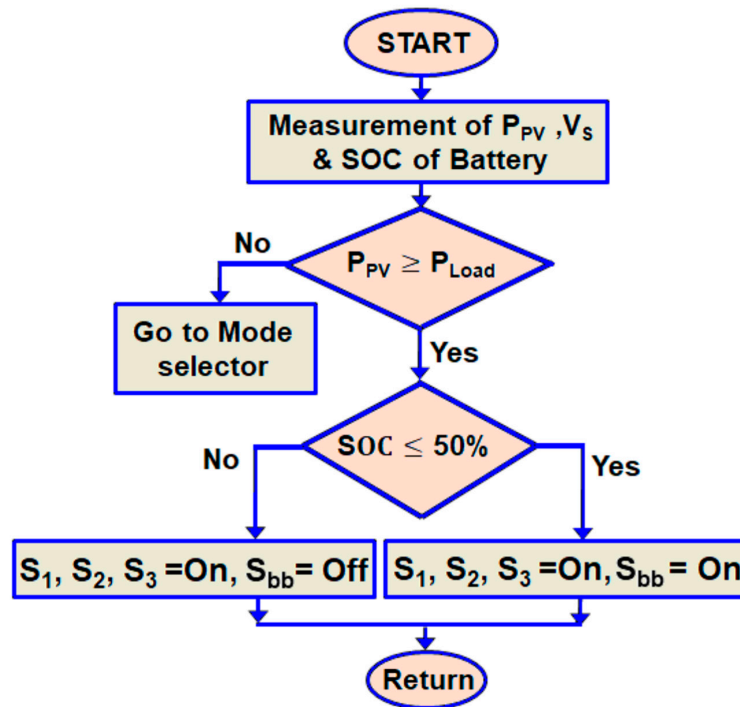


Figure 3. Flowchart for Mode 1.

4.2. Mode: 2

The power quality compensation mode is selected by the mode selector when the power provided by the PV system (P_{PV}) is less than or equal to the power required by the load (P_{Load}), and the SOC of the battery is less than or equal to 50%. The current-based compensation in this mode is achieved and power is supplied from the grid by activating switches S_1 , S_2 , S_3 , and S_{bb} . Figure 4 shows the flowchart for Mode 2.

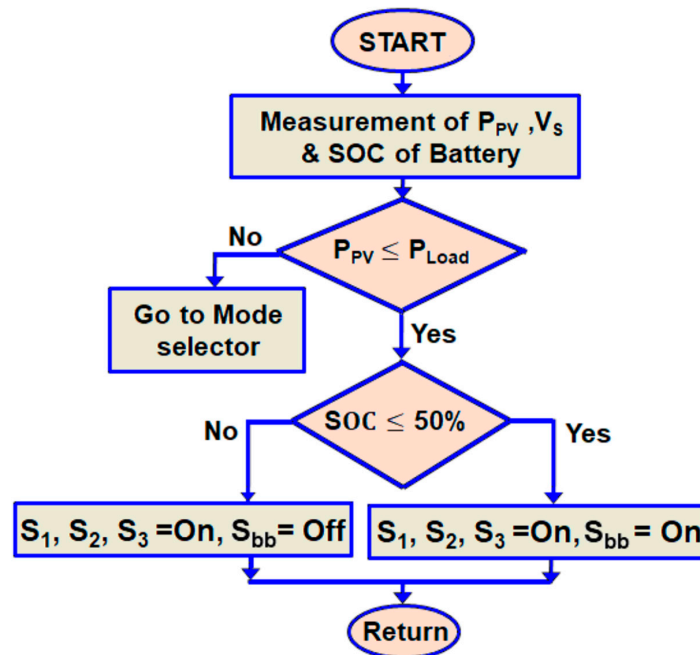


Figure 4. Flowchart for Mode 2.

4.3. Mode: 3

If the PV power (P_{PV}) is less than or equal to 50%, the mode selection will be chosen for the STATCOM compensation mode. This operational mode effectively offsets the current-based compensation and electricity received from the grid via the activation of switches S_1 , S_2 , and S_3 while simultaneously deactivating switch S_{bb} . Figure 5 shows the flowchart for Mode 3.

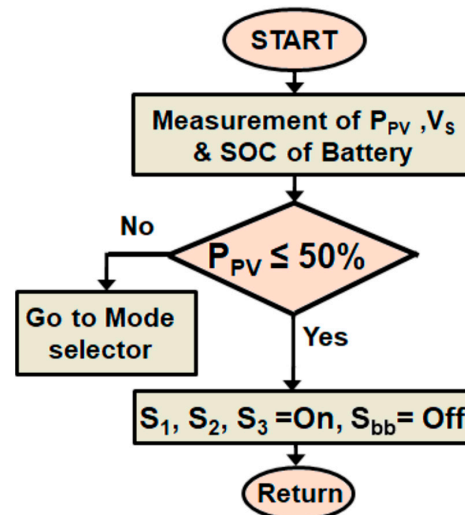


Figure 5. Flowchart for Mode 3.

4.4. Mode: 4

The PV system is now actively powering the load if V_{sabc} is less than 10% of the nominal supply voltage ($V_{sabc} = 400$ V) and P_{PV} is more than or equal to 80%, at which point the switches S_1 , S_2 , and S_3 are shut off to isolate the grid. The battery provides active power to the load by isolating the grid by turning off the switches S_1 , S_2 , and S_3 and switching on S_{bb} when P_{PV} production is below 20% and the SOC of the battery is more than 60%. Figure 6 shows the flowchart for Mode 4.

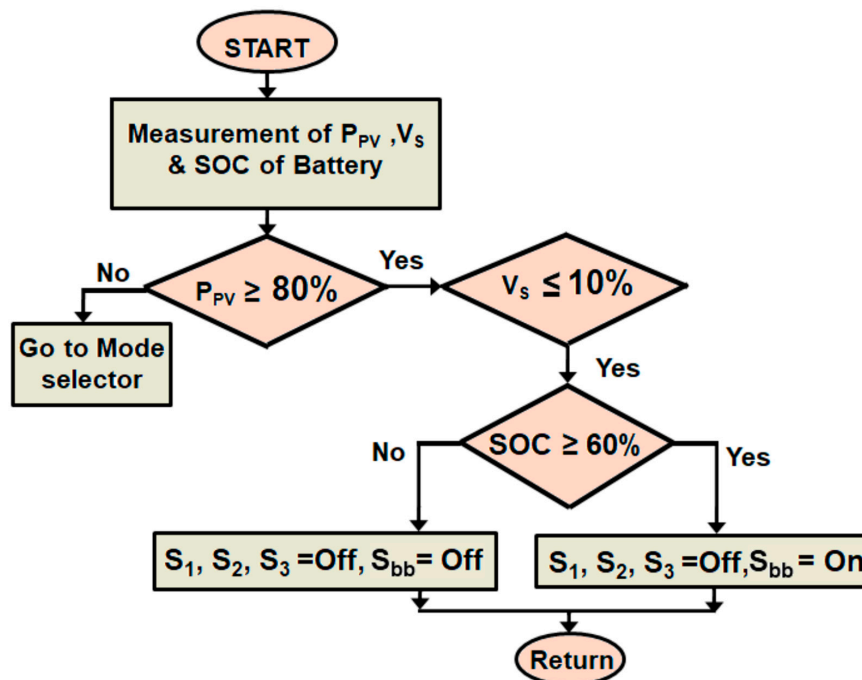


Figure 6. Flowchart for Mode 4.

reactive power controllers. The open loop transfer function of a (PLL) with a PI controller may be expressed as:

$$H_{PLL}(s) = \frac{\hat{V} \times k_{PLL,gain}}{T_f} \left(\frac{s + z_{PLL}}{s + T_f^{-1}} \right) \frac{1}{s^2} \quad (2)$$

The parameters k_{PLL} , gain, and Z_{PLL} refer to the controller parameters of a PLL. The use of the symmetrical optimum approach is employed to design the PI controller, ensure a phase margin of $\delta_m = 60^\circ$ at the cross-over frequency. The value of the variable ω_c is equal to 268 radians per second. Parallel loops are utilized in the MDNESOGI filter that has been presented to extract the third and fifth harmonics, which are then subtracted from the input signal, as seen in the block diagram that has been displayed in Figure 8. When dominant harmonics are removed, the prime loop is not subjected to as much filtering load, which improves the filter’s operating performance [30].

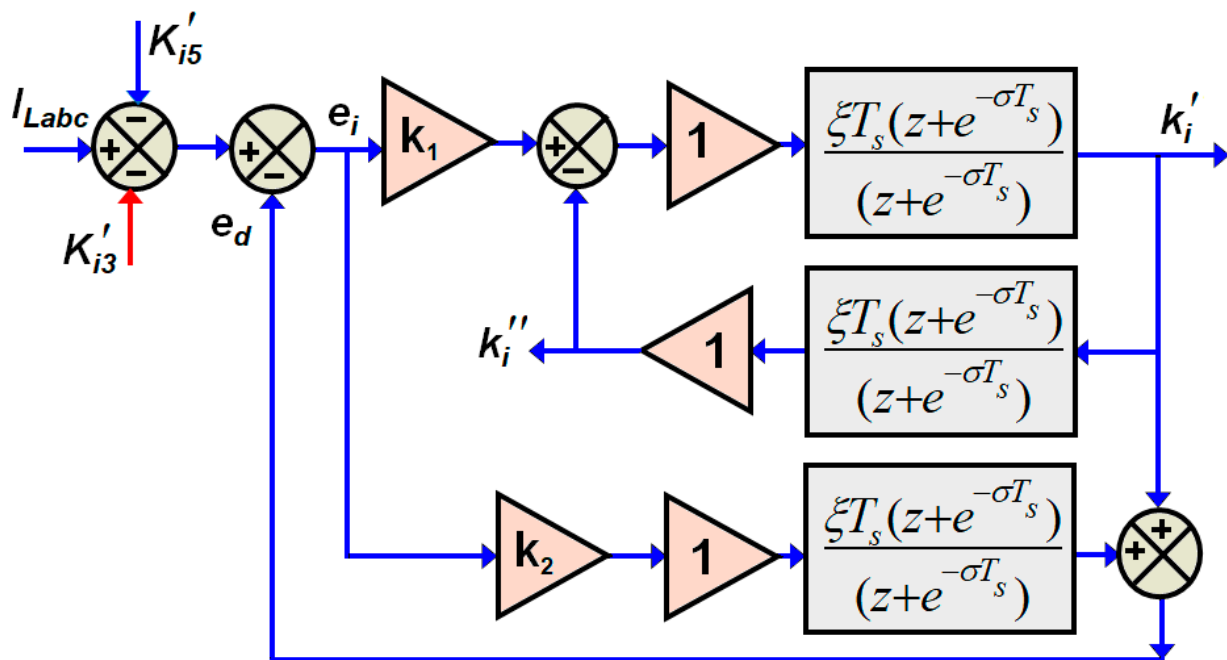


Figure 8. MDNESOGI internal block.

5.1. Current Control Scheme

In the dq frame of the inverter, the following currents are considered to be present:

$$L_f \frac{di_{id}}{dt} = L_f \omega(t) i_{iq} - R_f i_{id} + V_{id} - V_{pcc-d} \quad (3)$$

$$L_f \frac{di_{iq}}{dt} = L_f \omega(t) i_{id} - R_f i_{iq} + V_{iq} - V_{pcc-q} \quad (4)$$

The voltages of the PCC, the inverter current, and the voltage at the AC side of the inverter in the dq -frame are represented by the variables $V_{pcc,dq}$, $i_{i,dq}$, and $V_{i,dq}$, respectively, throughout the dq -frame. When it comes to the regulation of each current component, a PI controller is used. The inverter in the dq -frame exhibits active and reactive power outputs.

$$P_i(t) = \frac{3}{2} (V_{id}(t) i_{id}(t) + V_{iq}(t) i_{iq}(t)) \quad (5)$$

$$Q_i(t) = \frac{3}{2} (-V_{id}(t) i_{iq}(t) + V_{iq}(t) i_{id}(t)) \quad (6)$$

The PLL process causes V_{id} to equal \hat{V} and V_{iq} to be 0. As a result, the inverter's active power output may be regulated via the use of i_{id} , while the management of reactive power output is achieved by using i_{iq} . The present controllers get their reference values from outer loops, which are determined by the control goals and operating mode.

5.2. DC Link Voltage Control

The power loss caused by the inverter IGBT switches is made up of the actual power supplied by the DC link capacitor. As a result, there is a progressive decrease in the DC link capacitor voltage. In order to maintain the DC link capacitor charged, the inverter must draw a tiny amount of active power. The smart inverter control takes a very little amount of DC electricity from the solar panels in order to maintain the capacitor's charge [31]. This is in contrast to the fact that the bulk of the energy that is generated by solar panels is transmitted into the grid. The following is an example of the open loop transfer function related to the regulation of DC link voltage via the use of a PI controller:

$$H_{dc}(s) = \frac{3 \times V_{pcc-d} \times k_{dc,gain}}{2 \times \sigma_{i,d}} \left(\frac{s + z_{dc}}{s + \sigma_{i,d}^{-1}} \right) \frac{1}{s^2} \quad (7)$$

It is important to note that the parameters of the DC link voltage controller are k_{dc} , $gain$, and z_{dc} . A phase margin of 50° is employed in the design of this controller, which has a frequency of $\omega_c = 364$ rad/s.

5.3. AC Voltage Control

Taking into account the steady state behaviour of the PLL, using the assumptions that ($\varphi = \omega_0 t + \theta_0$) and $\omega = \omega_0$ and ignoring the small current flowing through the shunt filter capacitor, define the point of common coupling (PCC) voltage as follows:

$$V_{dc-d} = -L_g \omega_0 i_{iq} + L_g \omega_0 i_{Lq} - L_g \frac{di_{id}}{dt} + L_g \frac{di_{Ld}}{dt} + \hat{V} \quad (8)$$

The load current components in the d - q frame are denoted as $i_{L,d}$ and $i_{L,q}$. Inverter current control relies on the reference for the reactive component, which is made possible by the voltage control loop. Here is the AC voltage regulation's open loop transfer function:

$$H_{ac}(s) = \frac{k_{gain,ac}}{s} \times G_{iq}(s) \times (-L_g \omega_0) \quad (9)$$

$$H_{ac}(s) = \frac{-L_g \omega_0 k_{gain,ac}}{s(1 + \sigma_{i,q}s)} \quad (10)$$

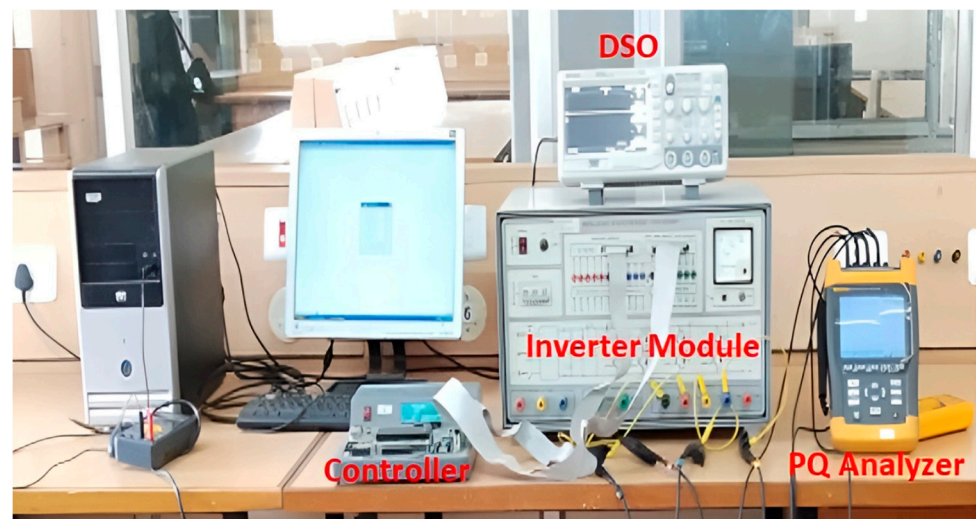
The AC voltage control loop is comprised of an inner loop, namely the current control loop. Consequently, the outer control loop must operate at a lower speed than the inner loop. Furthermore, if the current control loop exhibits a quicker response time compared to the AC voltage control loop, it is permissible to exclude the influence of the d -axis dynamics as a feed-forward component.

6. Experimental Results and Discussion

The MDNESOGI-based current and voltage controller method for the photovoltaic-assisted qZSI-STATCOM is evaluated in this study through an experimental prototype. Table 3 shows the system parameters used for the experimental prototype. The three separate scenarios that have been investigated in this experimental study are as follows: (1) balanced voltages with unbalanced loads; (2) balanced voltages with unbalanced loads; and (3) distorted voltage with unbalanced loads. Before and after the application of the compensator, the results of the experiments are shown. The experimental prototype image is shown in Figure 9.

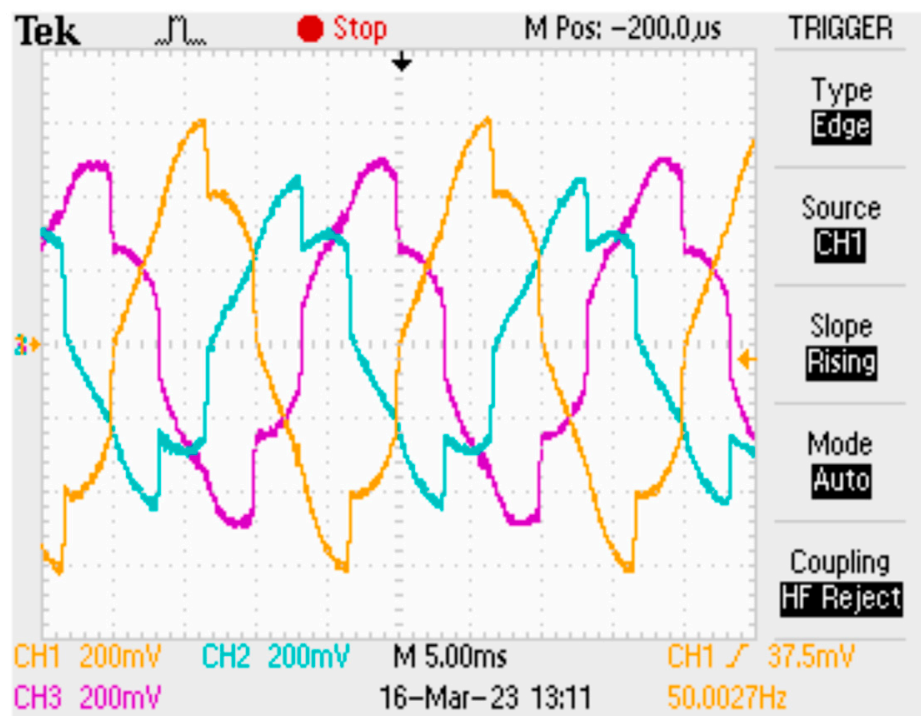
Table 3. System parameters of an experimental prototype.

Parameter	Rating	Symbol
Nominal voltage	400 V, 230 V	V_L, V_{ph}
Frequency of the system	50 Hz	f
STATCOM		
Filter inductance	26 mH	L_f
Resistance	1.5 Ω	R_f
Switching frequency	10 kHz	f_s
IGBT	600 V, 20 A, reactive power range: 2000 kVAR	
MOSFET	60 A, 300 V	
Gate Driver	LM5112	
Voltage-Current Sensor	Maximum sample rate: 1 kHz Voltage Range: ± 10 V	
Battery		
Battery capacity	500 Ah	Ah
PV Array		
Power output of PV array	400 w	PV_w
PV nominal voltage	72 V	V_{PV}
Voltage Doubler		
Inductance	48 μ H	L_{db}
Capacitance	3.151 μ F, 1.062 μ F, 1000 μ F	C_{db}, C_{db}, C_{out}
Switching frequency	20 kHz	f_{sD}

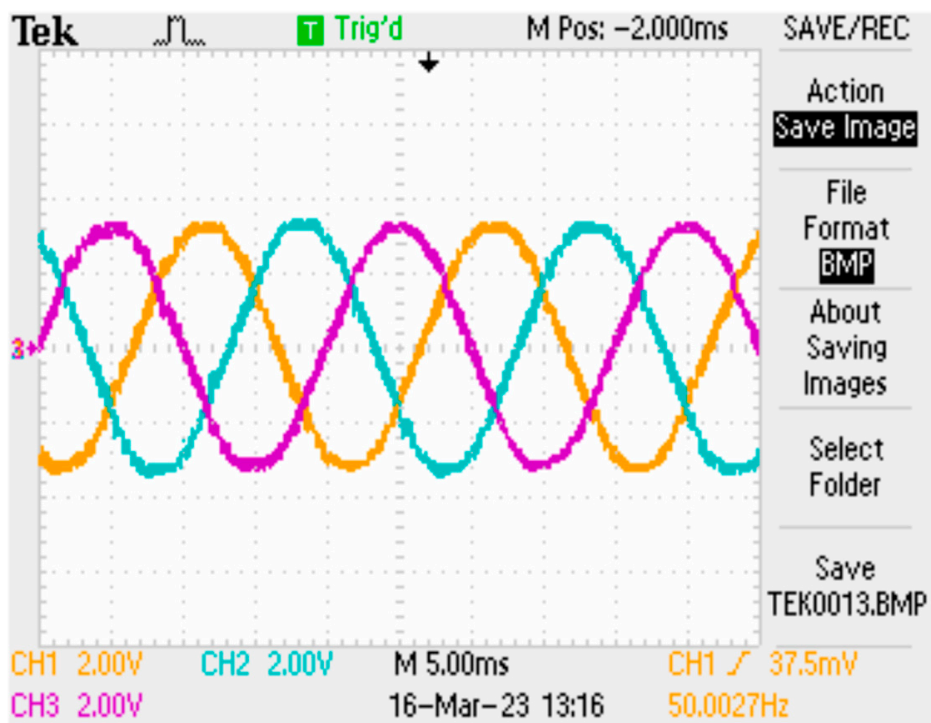
**Figure 9.** Experimental prototype image.

6.1. Case 1: Balanced Voltages with Unbalanced Loads

The distribution system is subjected to the balanced supply voltage as well as the unbalanced load in this instance. The results of current compensation experiments with balanced and unbalanced loads are shown in Figure 10. The experiments included measuring the load current before and after the PV-based qZSI-STATCOM was deployed, as well as the source current and voltage after compensation.

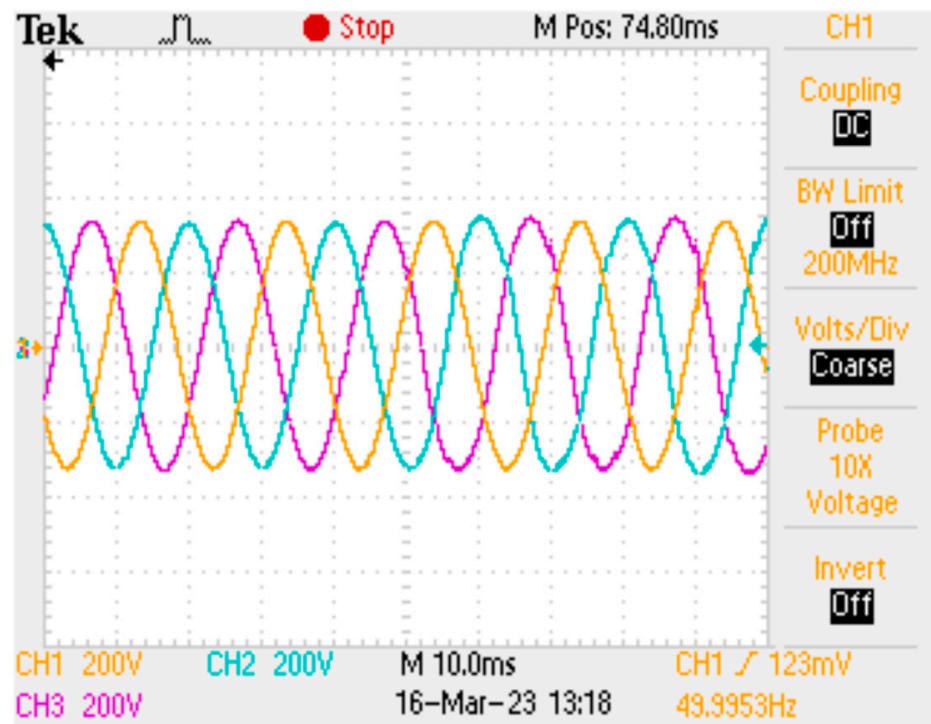


(a)

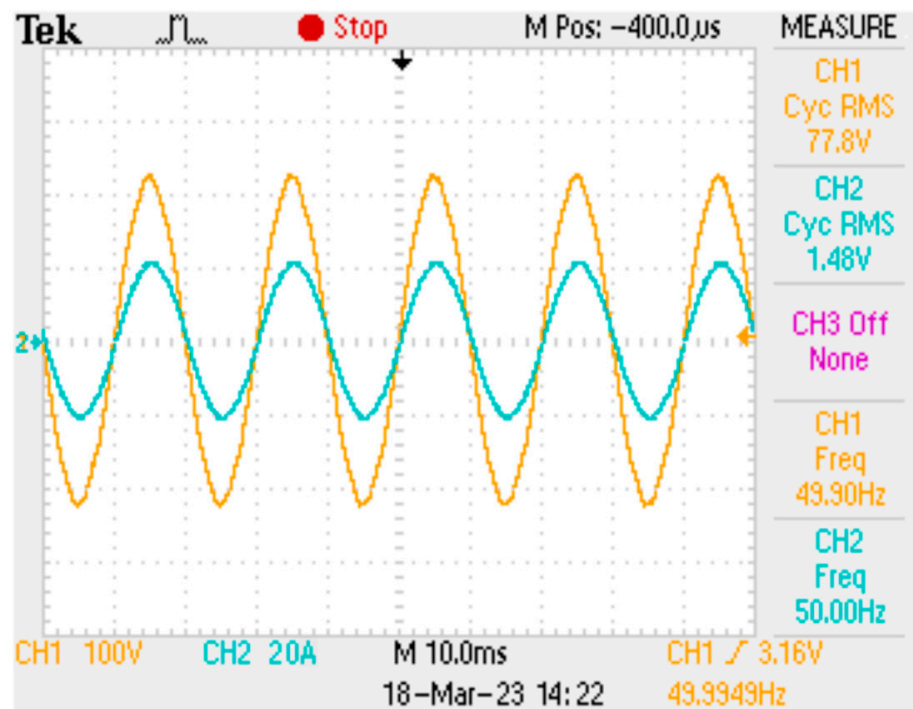


(b)

Figure 10. Cont.



(c)

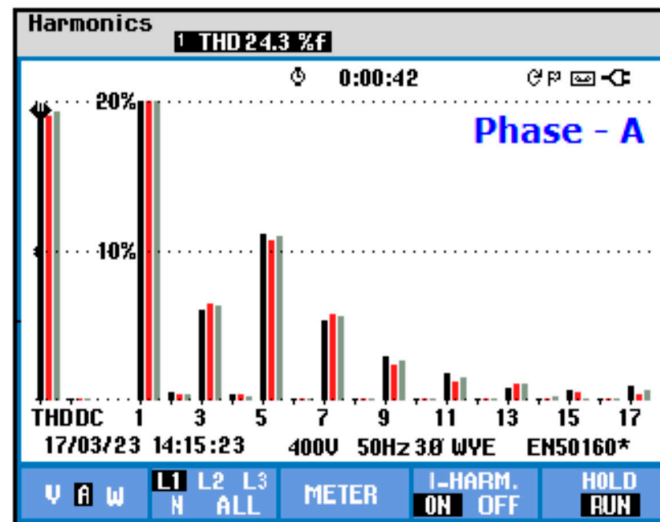


(d)

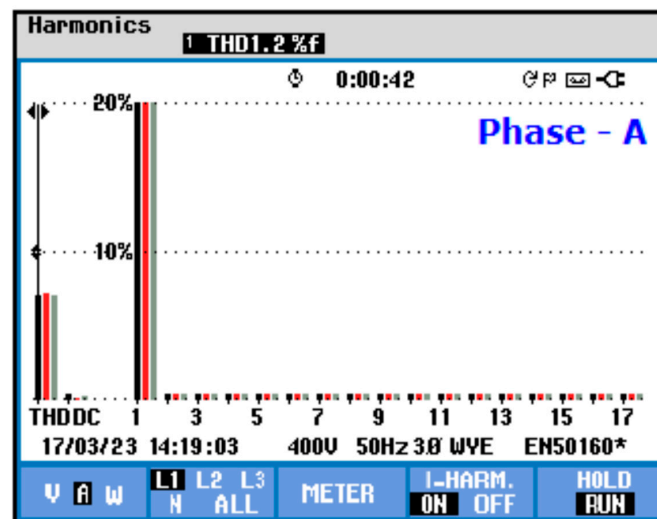
Figure 10. Results of current compensation experiments: (a) load current before the deployment of PV-based qZSI-STATCOM; (b) source current after the deployment of qZSI-STATCOM; (c) utility voltage; and (d) utility voltage and current.

Harmonic analysis of the load and source current prior to and after alleviating harmonics and in the three-phase distribution system is shown in Figure 11. The three-phase load currents were measured with THDs of 24.3%, 24.4%, and 24.3% before correction.

Source current THD levels were measured after adjustment to be about 1.2(%), 1.2(%) and 1.2(%) all of which are far lower than the limit set by IEEE Std. of 519-1992 [32]. European Standard EN 50160 on voltage characteristics of electricity supplied by public distribution networks [33].



(a)

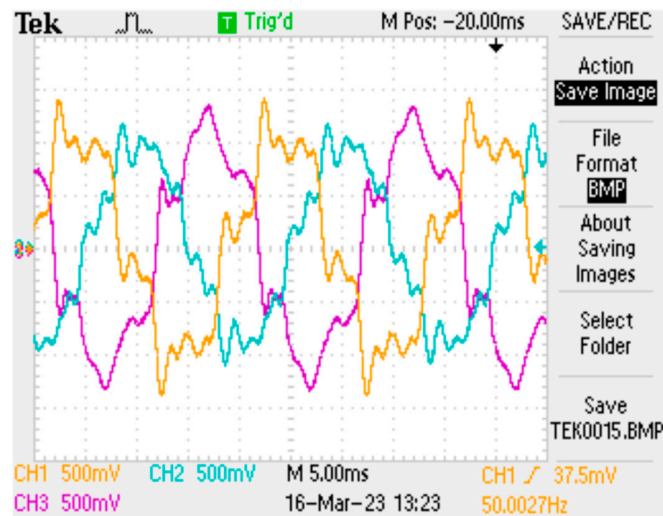


(b)

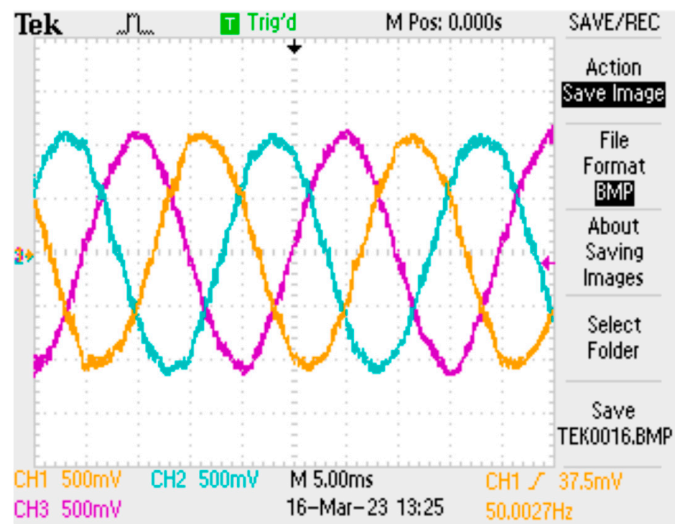
Figure 11. Harmonic spectrum for before and after compensation. (a) Load current harmonics prior compensation; (b) source current harmonics after compensation. (*): setups that are also valid for measuring mode Dips & Swells. Black, Red and Grey color indicates the A, B and C Phases respectively.

6.2. Case 2: Unbalanced Voltages with Unbalanced Loads

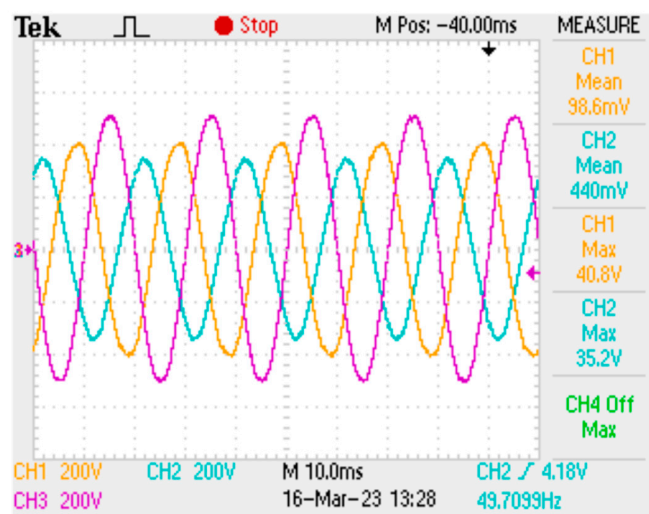
The operational efficiency of the PV-based qZSI-STATCOM is evaluated in this particular instance. The assessment takes place in the presence of unbalanced load situations as well as unbalanced voltage conditions. Figure 12 illustrates the experimental outcomes of current compensation in scenarios involving both unbalanced voltages and unbalanced loads. To be more specific, it displays the load current before the deployment of a PV-based q-ZSI-STATCOM, the source current after the deployment of the q-ZSI-STATCOM, and the source voltage prior to implementation.



(a)



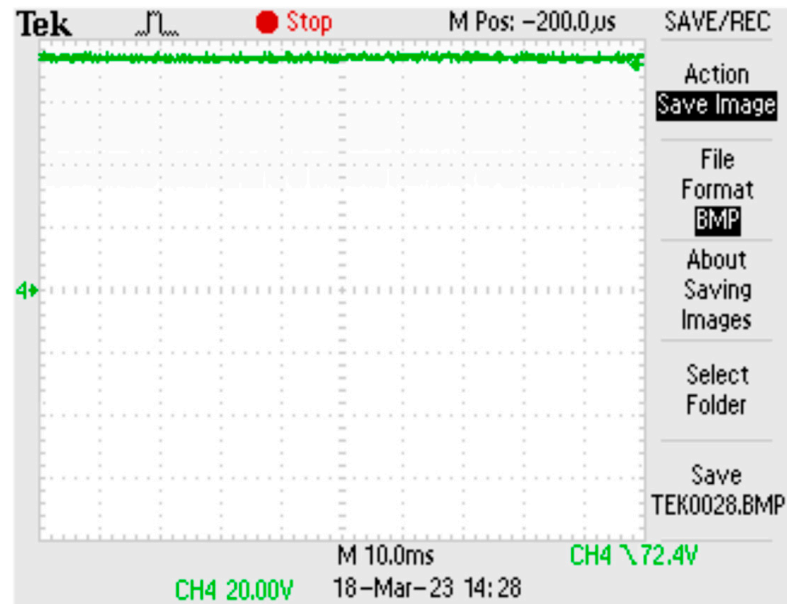
(b)



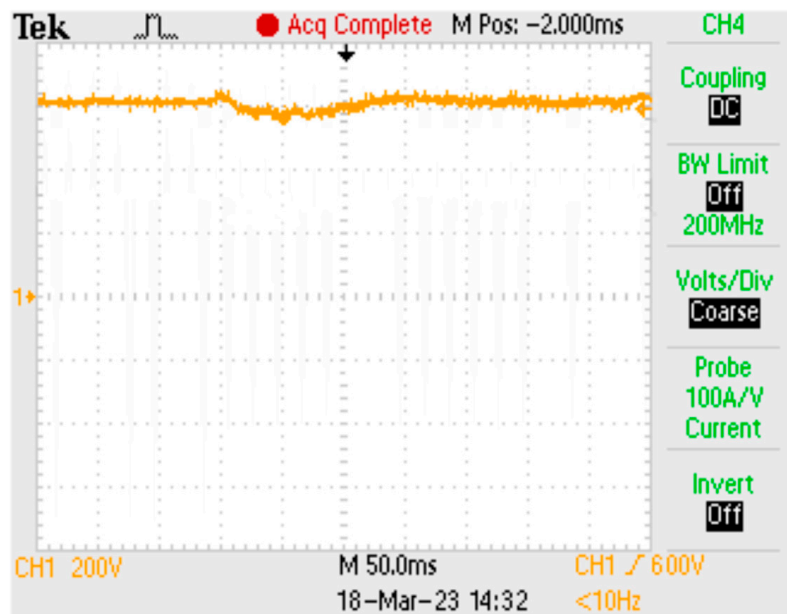
(c)

Figure 12. Experimental results of current compensation: (a) load current before implementation of qZSI-STATCOM; (b) source current after the deployment of qZSI-STATCOM; and (c) source voltage.

A representation of the PV array output voltage and the DC link voltage of the qZSI-STATCOM is shown in Figure 13. PV array voltage is given to the qZSI network, and it boosts the DC voltage magnitude to around 600 V.



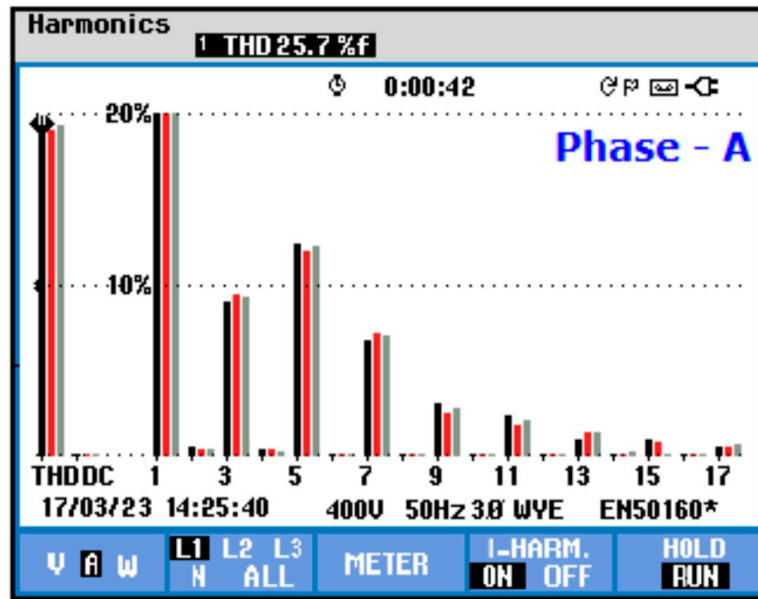
(a)



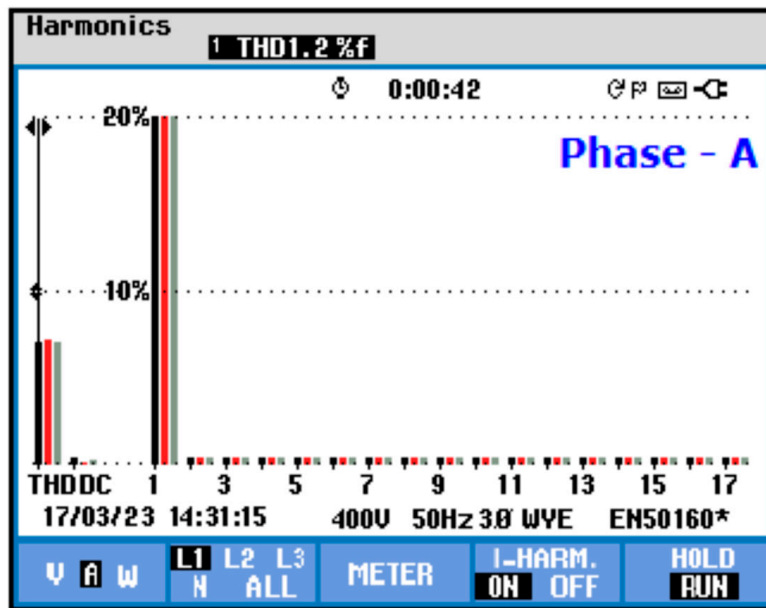
(b)

Figure 13. (a) PV array voltage; (b) DC link voltage of the qZSI-STATCOM.

Figure 14 depicts a harmonic analysis of the load and source current in a three-phase distribution system before and after harmonics were reduced. Before compensation, the THD of the three-phase load currents was 25.7%, 25.5%, and 25.6%, respectively. After making the necessary compensation, the THD values in the source current were measured to be about 1.2%, 1.2%, and 1.2%, respectively.



(a)

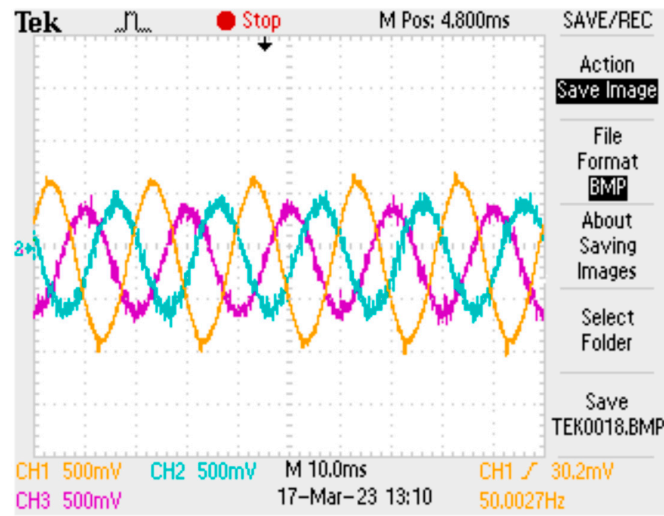


(b)

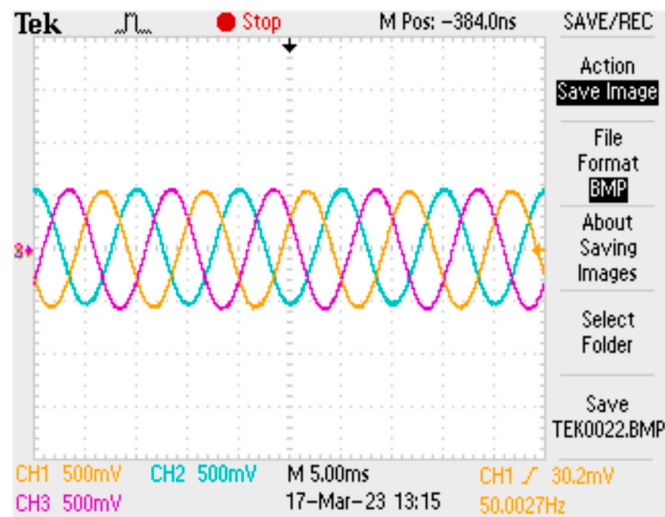
Figure 14. (a) Harmonic analysis of the load before harmonics compensation; (b) harmonic analysis of the source current after harmonics were reduced. (*): setups that are also valid for measuring mode Dips & Swells. Black, Red and Grey color indicates the A, B and C Phases respectively.

6.3. Case 3: Distorted Voltages with Unbalanced Loads

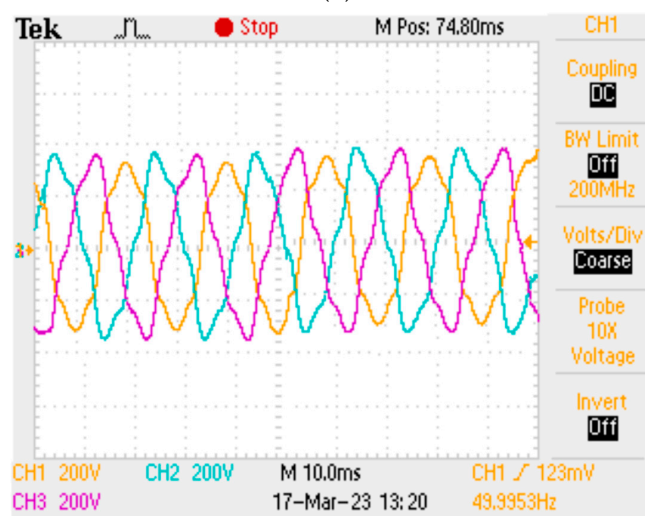
To assess the operational efficiency of the PV-based qZSI-STATCOM in the presence of distorted voltages and unbalanced loads, the previously unbalanced non-linear load is supplied with distorted AC voltages. The experimental results of current compensation under conditions of distorted voltages and unbalanced loads are shown in Figure 15. Figure 15 illustrates the load current, the source current following the deployment of the qZSI-STATCOM, the source voltage prior to the integration of the PV-based q-ZSI-STATCOM and the PV array, as well as the DC link voltage.



(a)

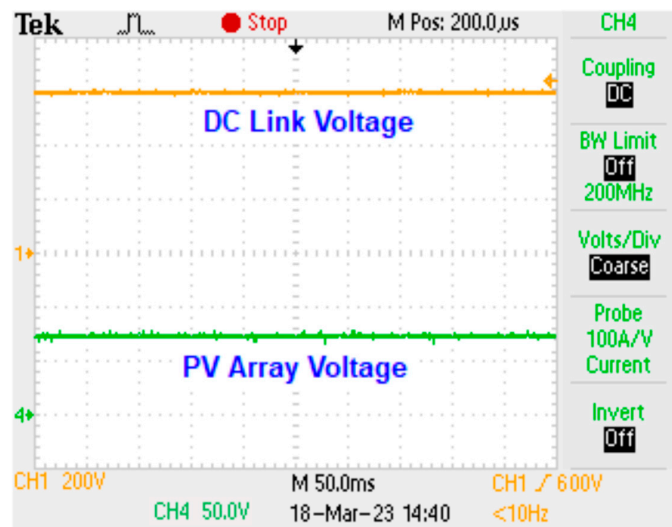


(b)



(c)

Figure 15. Cont.

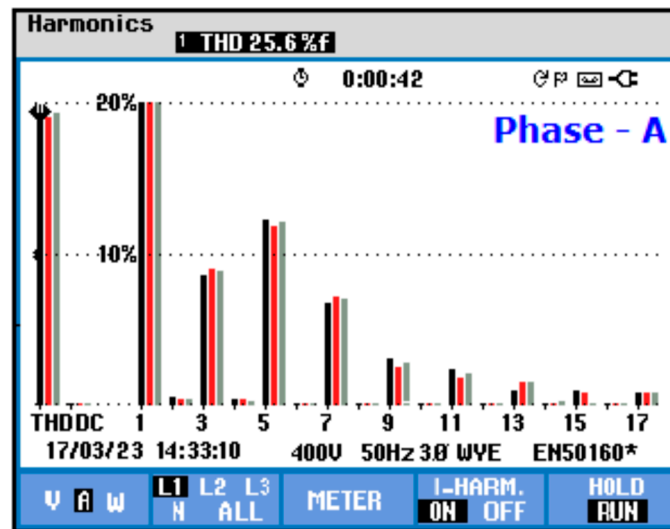


(d)

Figure 15. Experimental results of current compensation under case 3: (a) load current; (b) source current after the deployment of the qZSI-STATCOM; (c) Distorted source voltage; (d) PV array and DC-link voltage.

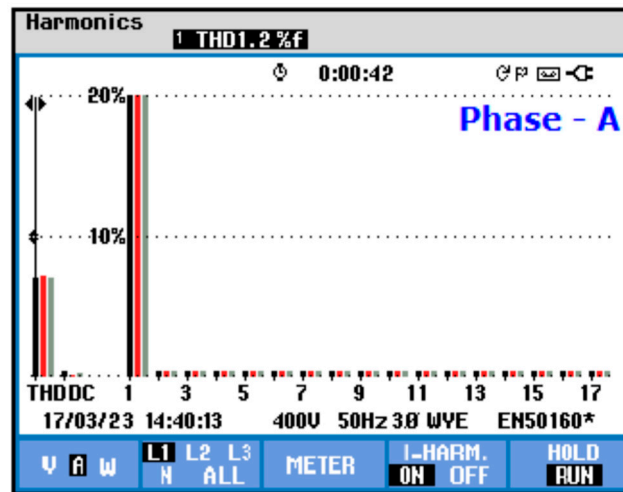
Figure 16 shows a harmonic analysis of the load and source current in a three-phase distribution system before and after harmonics compensation. Before compensation, the THDs of the three-phase load currents were 25.6%, 25.5%, and 25.5%, respectively. After making the necessary compensation, the THD values in the source current were measured to be about 1.2%, 1.2%, and 1.2%, respectively.

The experimental results for Operating Mode 1 are shown in Figure 17. The experimental results for Operating Mode 2 are shown in Figure 18.



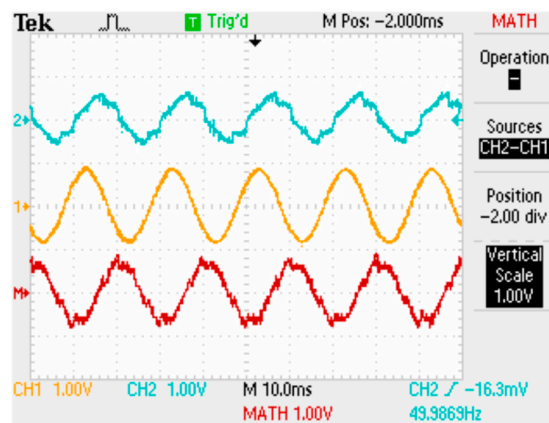
(a)

Figure 16. Cont.

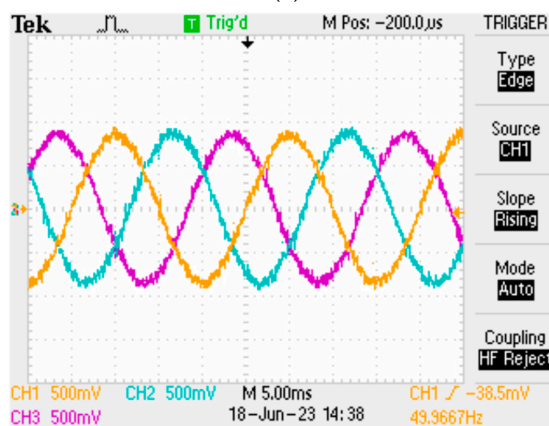


(b)

Figure 16. (a) Harmonic analysis of the load in a three-phase distribution system before harmonics compensation; (b) harmonic analysis of the source current in a three-phase distribution system after harmonics compensation. (*): setups that are also valid for measuring mode Dips & Swells. Black, Red and Grey color indicates the A, B and C Phases respectively.



(a)



(b)

Figure 17. Experimental results for Operating Mode 1: (a) source, injected, and compensation current; (b) three-phase source current after compensation.

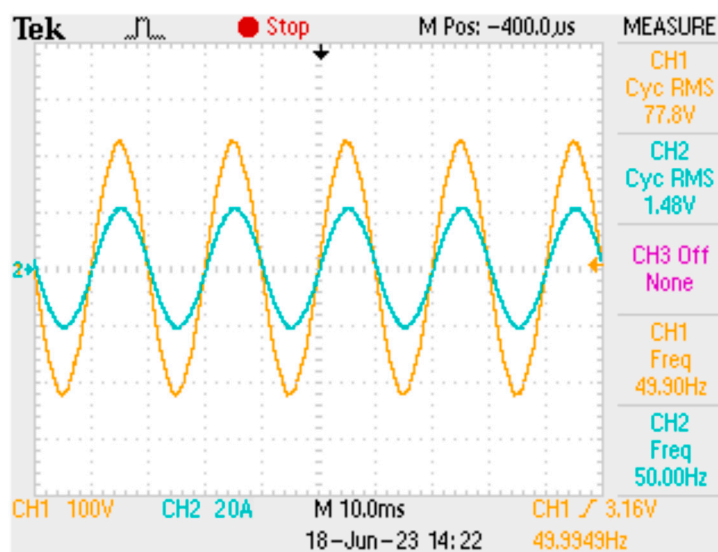


Figure 18. Experimental results for Operating Mode 2.

The experimental results for Operating Mode 3 are shown in Figure 19. Figure 19 shows the source current after compensation during Mode 3.

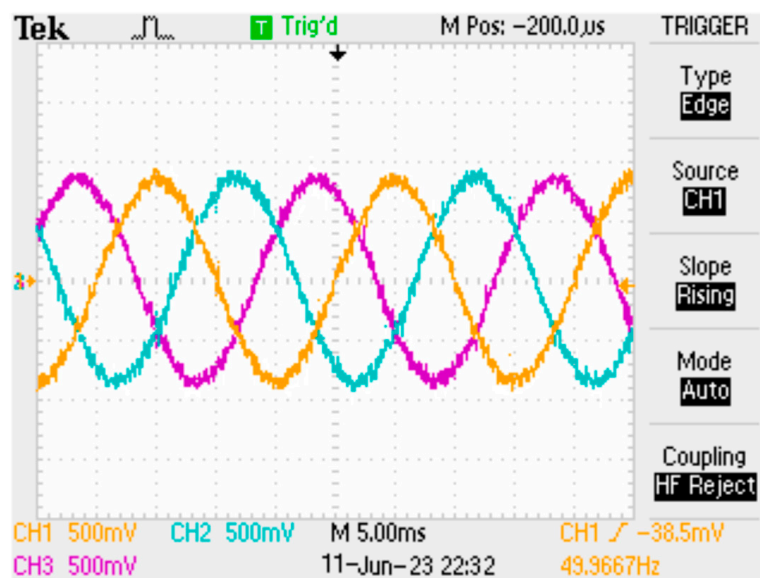
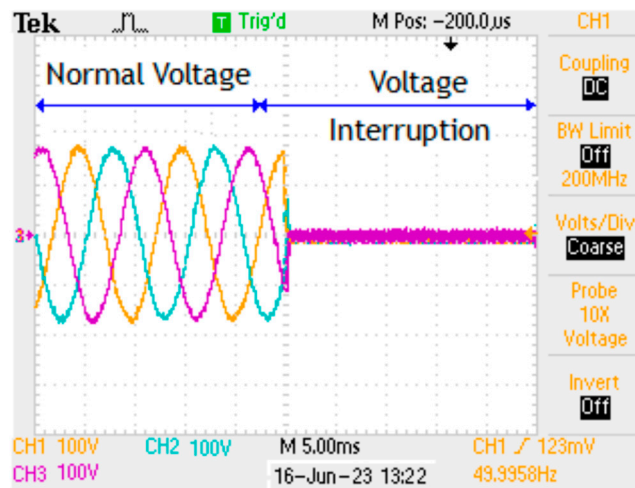


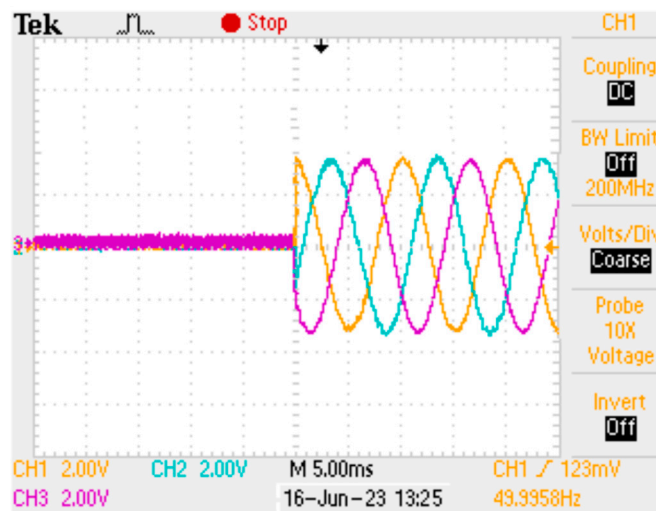
Figure 19. Experimental results for Operating Mode 3.

The experimental results for Operating Mode 4 are shown in Figure 20. Figure 20 shows the source voltage during voltage interruption, compensation voltage, and source voltage after compensation.

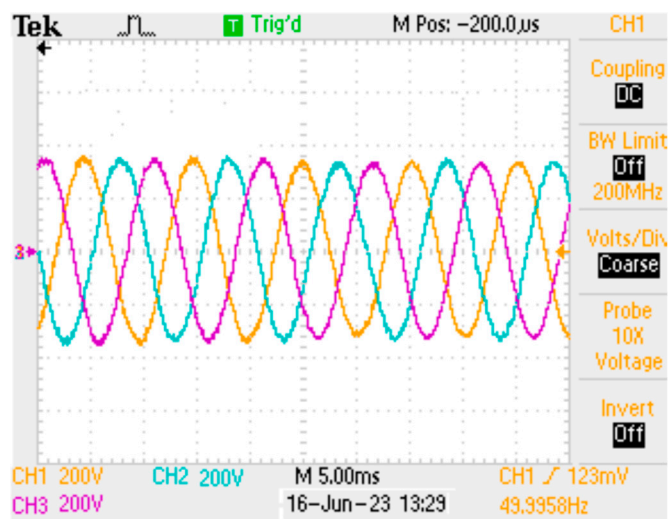
In addition to reducing the load current harmonics and compensating for reactive power, the photovoltaic-based qZSI DSTATCOM serves the purpose of smoothing the transfer of electricity from the PV system to the grid. Table 4 provides a concise overview of the findings of the PV- qZSI-STATCOM's efforts to compensate for harmonic distortion.



(a)



(b)



(c)

Figure 20. Experimental results for Operating Mode 4: (a) source voltage during voltage interruption, (b) compensation voltage, (c) source voltage after compensation.

Table 4. Harmonic compensation results of PV-qZSI- STATCOM.

Case Study	THD Results of Experimentation					
	Before Compensation THD (%)			After Compensation THD (%)		
	Phase-A	Phase-B	Phase-C	Phase-A	Phase-B	Phase-C
1	24.3	24.4	24.3	1.2	1.2	1.2
2	25.7	25.5	25.6	1.2	1.2	1.2
3	25.6	25.5	25.5	1.2	1.2	1.2

7. Performance Comparison of Proposed and Conventional Controllers

Table 5 presents a comparison of the findings that were presented in this research with the findings of some other studies that were published in the literature and that were similar to the findings presented in this investigation. The best-case scenario is considered to be the case to facilitate the comparison of the THDs in currents during dynamic operations. It is obvious that the grid-integrated PV energy system that was given with support from STATCOM either outperforms a large number of other hybrid RES system schemes or reaches levels of performance that are comparable to those that have been detailed in the study that has been published. A FACTS controller is crucial in grid-integrated hybrid systems, as this shows. This provides an attractive strategy in addition to a high-quality solution for dealing with the many performance issues that arise in these hybrid systems.

Table 5. Performance analysis of proposed control strategy and existing control strategy.

Control Strategy	THD (%)	Proficiency of DC Offset Rejection	Steady-State Error	Compensation Capability	Power Loss	Energy Source/Energy Storage
Proportional Resonant (PR) Controller [34]	4.2	No	Slow	Short-term	High	Capacitor
Voltage Oriented Control [35]	6.20	Less Rejection	Moderate	Short-term	Moderate	Capacitor
Direct Power Control [35]	3.17	No	Moderate	Short-term	Moderate	Capacitor
JAYA Algorithm [36]	3.0	No	Moderate	Short-term	Moderate	Battery
Proposed Control Scheme	1.2	More rejection	Quick response	Long-term	Low	PV/Battery

The THD analysis of the conventional and suggested control schemes is shown in Figure 21. The suggested MDNESOGI control scheme demonstrates greater compensatory capabilities according to the THD results.

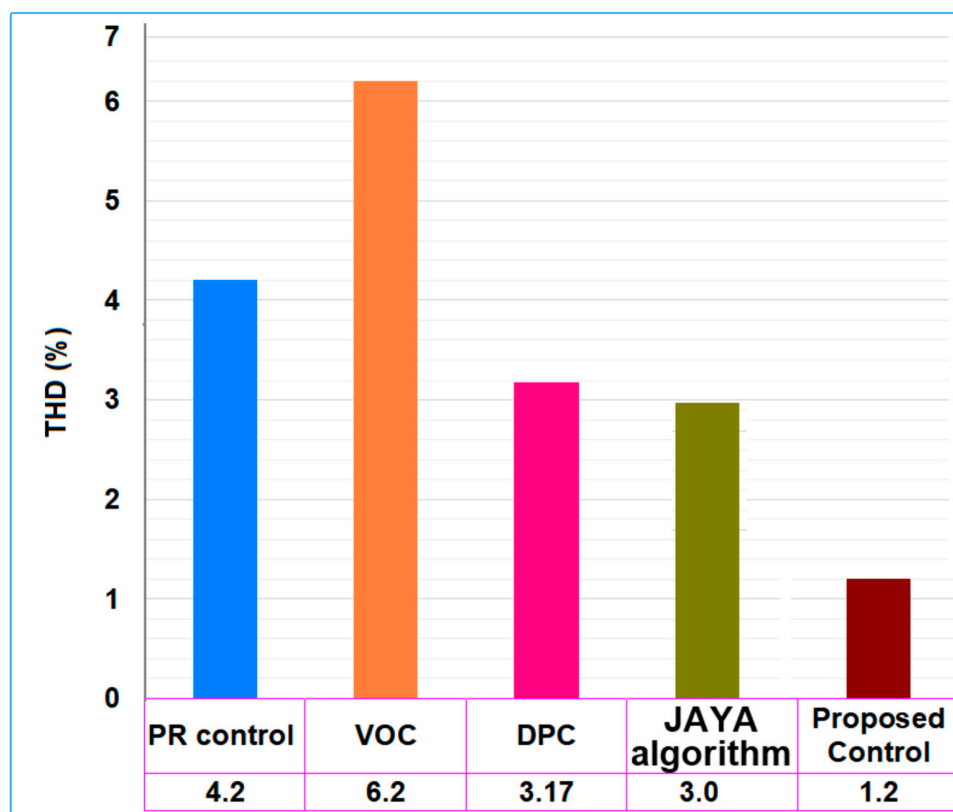


Figure 21. THD analysis of conventional and proposed control scheme.

8. Conclusions

This study presents a control structure that utilizes MDNESOGI to generate the inverter reference current needed for determining the requisite harmonic content. By using basic mathematical processes, the proposed structure has been constructed in a manner that drastically reduces the time required for sampling to an incredibly manageable level. This allows for a more commendable dynamic response by increasing the reference current generation speed to an acceptable level. To conform to the IEEE standard, the source current wave shape has been improved due to the controller that was presented, and the THD level has been reduced to well below 5%. In addition, this structure has proven useful in real-world situations by providing load balancing, reactive power compensation, PCC voltage control, and DC link voltage control. Additionally, a comparative study has been provided to indicate that a controller based on MDNESOGI is superior to controllers based on SOGI and improved SOGI in terms of cost, the elimination of harmonics, the need for fewer computations, and the elimination of DC offset. This is demonstrated by the fact that the controllers are based on MDNESOGI. Consequently, it is feasible to arrive at the suitable conclusion that the proposed controller has a structure that is much less complicated, very robust, and highly effective in terms of reducing harmonics, voltage levels, and DC offsets across a broad range of operating scenarios. This result may be reached because it is possible to arrive at the proper conclusion.

Author Contributions: Conceptualization, K.N.; Methodology, V.M.; Software, V.M.; Validation, R.M.; Formal analysis, R.M.; Investigation, K.N.; Resources, O.A.; data curation, V.M.; writing—original draft preparation, V.M.; writing—review and editing, K.N.; visualization, O.A.; supervision, K.N.; project administration, K.N.; funding acquisition, K.N. All authors have read and agreed to the published version of the manuscript.

Funding: The authors extend their appreciation to the Deputyship for Research and Innovation, Ministry of Education in Saudi Arabia for funding this research work through the project number IF2-PSAU/2022/01/22797.

Data Availability Statement: Data are contained within the article.

Conflicts of Interest: The authors declare no conflicts of interest.

References

1. Srivastava, M.; Goyal, S.K.; Saraswat, A.; Shekhawat, R.S.; Gangil, G. A Review on Power Quality Problems, Causes and Mitigation Techniques. In Proceedings of the 2022 1st International Conference on Sustainable Technology for Power and Energy Systems (STPES), Srinagar, India, 4–6 July 2022; pp. 1–6. [\[CrossRef\]](#)
2. Bollen, M.H. *Understanding Power Quality Problems-Voltage Sags and Interruptions*; IEEE Press: New York, NY, USA, 2000. [\[CrossRef\]](#)
3. Gao, M.; Awodele, K. Investigation of power electronics solutions to power quality problems in distribution networks. In Proceedings of the AFRICON 2015, Addis Ababa, Ethiopia, 14–17 September 2015; pp. 1–6. [\[CrossRef\]](#)
4. Sepasi, S.; Talichet, C.; Pramanik, A.S. Power Quality in Microgrids: A Critical Review of Fundamentals, Standards, and Case Studies. *IEEE Access* **2023**, *11*, 108493–108531. [\[CrossRef\]](#)
5. Ezhiljenekha, B.; MarsalineBeno, M. Review of Power Quality Issues in Solar and Wind Energy. *Mater. Today Proc.* **2020**, *24*, 2137–2143. [\[CrossRef\]](#)
6. Gupta, A. Power quality evaluation of photovoltaic grid interfaced cascaded H-bridge nine-level multilevel inverter systems using D-STATCOM and UPQC. *Energy* **2022**, *238*, 121707. [\[CrossRef\]](#)
7. Houran, M.A.; Sabzevari, K.; Hassan, A.; Oubelaid, A.; Tostado-Véliz, M.; Khosravi, N. Active power filter module function to improve power quality conditions using GWO and PSO techniques for solar photovoltaic arrays and battery energy storage systems. *J. Energy Storage* **2023**, *72*, 108552. [\[CrossRef\]](#)
8. Harirchi, F.; Simões, M.G. Enhanced Instantaneous Power Theory Decomposition for Power Quality Smart Converter Applications. *IEEE Trans. Power Electron.* **2018**, *33*, 9344–9359. [\[CrossRef\]](#)
9. Han, Y.; Fang, X.; Yang, P.; Wang, C.; Xu, L.; Guerrero, J.M. Stability Analysis of Digital-Controlled Single-Phase Inverter with Synchronous Reference Frame Voltage Control. *IEEE Trans. Power Electron.* **2018**, *33*, 6333–6350. [\[CrossRef\]](#)
10. Yallamilli, R.S.; Mishra, M.K. Instantaneous Symmetrical Component Theory Based Parallel Grid Side Converter Control Strategy for Microgrid Power Management. *IEEE Trans. Sustain. Energy* **2019**, *10*, 682–692. [\[CrossRef\]](#)
11. Liang, X. Emerging Power Quality Challenges Due to Integration of Renewable Energy Sources. *IEEE Trans. Ind. Appl.* **2017**, *53*, 855–866. [\[CrossRef\]](#)
12. Azbe, V.; Mihalic, R. STATCOM control strategies in energy-function-based methods for the globally optimal control of renewable sources during transients. *Int. J. Electr. Power Energy Syst.* **2022**, *141*, 108145. [\[CrossRef\]](#)
13. Patel, N.; Gupta, N.; Babu, B.C. Photovoltaic system operation as DSTATCOM for power quality improvement employing active current control. *IET Gener. Trans. Distrib.* **2020**, *14*, 3518–3529. [\[CrossRef\]](#)
14. Badoni, M.; Singh, A.; Singh, B. Comparative Performance of Wiener Filter and Adaptive Least Mean Square-Based Control for Power Quality Improvement. *IEEE Trans. Ind. Electron.* **2016**, *63*, 3028–3037. [\[CrossRef\]](#)
15. Singh, B.; Solanki, J. A Comparison of Control Algorithms for DSTATCOM. *IEEE Trans. Ind. Electron.* **2009**, *56*, 2738–2745. [\[CrossRef\]](#)
16. Liu, A.; Li, H. Stabilization of Delayed Boolean Control Networks with State Constraints: A Barrier Lyapunov Function Method. *IEEE Trans. Circuits Syst. II Express Briefs* **2021**, *68*, 2553–2557. [\[CrossRef\]](#)
17. Giri, A.K.; Arya, S.R.; Maurya, R.; Babu, B.C. VCO-Less PLL Control-Based Voltage-Source Converter for Power Quality Improvement in Distributed Generation System. *IET Electr. Power Appl.* **2019**, *13*, 1114–1124. [\[CrossRef\]](#)
18. Ram, A.; Sharma, P.R.; Ahuja, R.K. Enhancement of power quality using U-SOGI based control algorithm for DSTATCOM. *Ain Shams Eng. J.* **2023**, *2023*, 102296. [\[CrossRef\]](#)
19. Astero, P.; Söder, L. Improving PV Dynamic Hosting Capacity Using Adaptive Controller for STATCOMs. *IEEE Trans. Energy Convers.* **2019**, *34*, 415–425. [\[CrossRef\]](#)
20. Rashad, A.; Kamel, S.; Jurado, F.; Abdel-Nasser, M.; Mahmoud, K. ANN-Based STATCOM Tuning for Performance Enhancement of Combined Wind Farms. *Electr. Power Compon. Syst.* **2019**, *47*, 10–26. [\[CrossRef\]](#)
21. Zhang, G.; Hu, W.; Cao, D.; Yi, J.; Huang, Q.; Liu, Z.; Chen, Z.; Blaabjerg, F. A Data-Driven Approach for Designing STATCOM Additional Damping Controller for Wind Farms. *Int. J. Electr. Power Energy Syst.* **2020**, *117*, 105620. [\[CrossRef\]](#)
22. Kamel, O.M.; Diab, A.A.Z.; Do, T.D.; Mossa, M.A. A Novel Hybrid Ant Colony-Particle Swarm Optimization Techniques Based Tuning STATCOM for Grid Code Compliance. *IEEE Access* **2020**, *8*, 41566–41587. [\[CrossRef\]](#)
23. Bakir, H.; Kulaksiz, A.A. Modelling and Voltage Control of the Solar-Wind Hybrid Micro-grid with Optimized STATCOM Using GA and BFA. *Eng. Sci. Technol. Int. J.* **2020**, *23*, 576–584. [\[CrossRef\]](#)
24. Kumar, R.; Singh, R.; Ashfaq, H. Stability Enhancement of Induction Generator-Based Series Compensated Wind Power Plants by Alleviating Subsynchronous Torsional Oscillations Using BFOA-Optimal Controller Tuned STATCOM. *Wind Energy* **2020**, *23*, 1846–1867. [\[CrossRef\]](#)
25. Fatama, A.Z.; Khan, M.A.; Kurukuru, V.S.B.; Haque, A.; Blaabjerg, F. Coordinated Reactive Power Strategy Using Static Synchronous Compensator for Photovoltaic Inverters. *Int. Trans. Electr. Energy Syst.* **2020**, *30*, 1–18. [\[CrossRef\]](#)
26. Sonawane, A.J.; Umarikar, A.C. Voltage and Reactive Power Regulation with Synchronverter-Based Control of PV-STATCOM. *IEEE Access* **2023**, *11*, 52129–52140. [\[CrossRef\]](#)

27. Raja, A.; Vijayakumar, M.; Karthikeyan, C. Solar Photovoltaic Interconnected ZSI-Unified Power Quality Conditioner to Enhance Power Quality. *Bull. Pol. Acad. Sci. Tech. Sci.* **2022**, *70*, e140015. [[CrossRef](#)]
28. Muthuvel, K.; Vijayakumar, M. Solar PV Sustained Quasi Z-Source Network-Based Unified Power Quality Conditioner for Enhancement of Power Quality. *Energies* **2020**, *13*, 2657. [[CrossRef](#)]
29. Xie, M.; Wen, H.; Zhu, C.; Yang, Y. DC Offset Rejection Improvement in Single-Phase SOGI-PLL Algorithms: Methods Review and Experimental Evaluation. *IEEE Access* **2017**, *5*, 12810–12819. [[CrossRef](#)]
30. Varma, R.K.; Siavashi, E.M. PV-STATCOM: A New Smart Inverter for Voltage Control in Distribution Systems. *IEEE Trans. Sustain. Energy* **2018**, *9*, 1681–1691. [[CrossRef](#)]
31. Gawhade, P.; Ojha, A. Recent Advances in Synchronization Techniques for Grid-Tied PV System: A Review. *Energy Rep.* **2021**, *7*, 6581–6599. [[CrossRef](#)]
32. *IEEE Std. 519-1992*; IEEE Recommended Practices and Requirement for Harmonic Control on Electric Power System. IEEE Std.: New York, NY, USA, 1992; p. 519.
33. European Standard EN50160 (1999). Voltage Characteristics of Electricity Supplied by Public Distribution System. CENELEC: Brussels, Belgium, 1999.
34. Jahnvi, B.; Karanki, S.B.; Kar, P.K. Power Quality Improvement with D-STATCOM Using Combined PR and Comb Filter-Controller. In Proceedings of the 1st International Conference on Power Electronics and Energy (ICPEE), Bhubaneswar, India, 2–3 January 2021; pp. 1–6. [[CrossRef](#)]
35. Sayahi, K.; Kadri, A.; Bacha, F.; Marzougui, H. Implementation of a D-STATCOM Control Strategy Based on Direct Power Control Method for Grid Connected Wind Turbine. *Int. J. Electr. Power Energy Syst.* **2020**, *121*, 106105. [[CrossRef](#)]
36. Alvaro, R.; Águila Téllez, A.; Ortiz, L. Optimal Location and Sizing of a D-STATCOM in Electrical Distribution Systems to Improve the Voltage Profile Considering the Restriction of Harmonic Injection through the JAYA Algorithm. *Energies* **2023**, *16*, 7683. [[CrossRef](#)]

Disclaimer/Publisher’s Note: The statements, opinions and data contained in all publications are solely those of the individual author(s) and contributor(s) and not of MDPI and/or the editor(s). MDPI and/or the editor(s) disclaim responsibility for any injury to people or property resulting from any ideas, methods, instructions or products referred to in the content.